PHOTOINJECTOR EMITTANCE OPTIMIZATION USING LATENT LASER PULSE REPRESENTATIONS

A. Klemps*[1], N. Ay[1], P. K. Banerjee[1], Y. Chen[2], I. Hartl[2], D. Ilia[2], J. Kwasniok[2], H. Tünnermann[2]
[1]Hamburg University of Technology, Hamburg, Germany
[2]Deutsches Elektron-Synchrotron (DESY), Hamburg, Germany

Abstract

We present a beam dynamics study aimed at optimizing the transverse emittance of electron bunches in a photoinjector, motivated by the performance requirements of Free-Electron Lasers. The study is conducted using the accelerator configuration of the Photo Injector Test Facility at DESY in Zeuthen (PITZ), with the overarching goal of developing emittance optimization strategies for the European XFEL photoinjector. To this end, we perform large-scale beam dynamics simulations using the simulation code ASTRA, systematically sampling from a low-dimensional latent representation of temporal laser pulse profiles. This latent space is learned from a broad set of physically plausible pulses using a Wasserstein Autoencoder (WAE), enabling compact and structured exploration of pulse shape variations. The ability to efficiently sample from this representation supports targeted emittance studies that would be computationally prohibitive in the original high-dimensional shaping parameter space. For each simulation, beam quality metrics such as normalized projected emittance and slice mismatches are recorded. The study reveals meaningful correlations between latent coordinates and beam quality, demonstrating the utility of WAE-based representations in guiding laser pulse design. We briefly outline future directions involving neural surrogate models to accelerate beam emittance optimization.

INTRODUCTION

The performance of photoinjectors for Free-Electron Lasers (FELs) critically depends on the generation of electron beams with low transverse emittance. With the commissioning of the photocathode laser system NEPAL [1] at the European XFEL and PITZ, advanced temporal pulse shaping capabilities have become available, enabling the generation of laser pulses with diverse temporal profiles via precise control [2, 3] and opening up targeted emittance optimization studies at EuXFEL [4].

However, the underlying shaping process is governed by a high-dimensional parameter space with several thousand tunable degrees of freedom, making systematic exploration through beam dynamics simulations computationally prohibitive. At the same time, the relationship between temporal pulse shape and resulting transverse emittance remains difficult to characterize due to nonlinear space charge effects.

To this end, machine learning methods have recently been successfully applied to the modeling, control, and optimization of particle accelerators, enabling data-driven representations and predictions of complex beam dynamics such as space charge effects [5, 6].

In this work, we employ latent representations of temporal pulse shapes learned with Wasserstein Auto-Encoders [7], providing a compact, low-dimensional parametrization of physically admissible profiles. Based on samples from this latent space, we perform beam dynamics simulations of the PITZ injector and analyze the impact of longitudinal pulse shaping on transverse emittance.

LATENT PULSE REPRESENTATIONS

WAEs are a class of generative models with a training objective derived from optimal transport theory, enabling well-regularized latent representations and accurate reconstruction of input data. In prior work [8], we trained a convolutional WAE on simulated laser pulse data [9], representing physically admissible temporal profiles generated by the NEPAL pulse-shaping system. The trained model maps each pulse shape given in time domain to a low-dimensional latent representation $\xi \in \mathbb{R}^{32}$, providing a compact alternative to the approximately 6 000 tunable parameters of the spatial light modulator (SLM) used for pulse shaping. This dimensionality reduction enables an efficient parametrization of the pulse space while retaining physically relevant pulse structure.

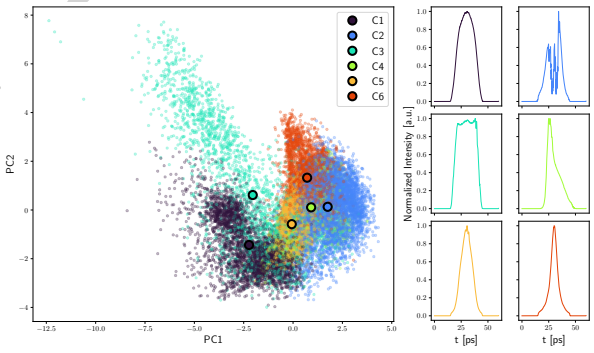

Figure 1: PCA projection of the WAE latent space with Gaussian mixture clustering. Circles denote component means; right panels show decoded mean pulse shapes.

The learned latent space is smooth and structured, clustering pulse shape families (Fig. 1) and enabling physically plausible interpolations. In contrast, the original shaping parameter space is governed by a complex nonlinear optical process not directly accessible in beam dynamics studies. The latent variables therefore provide an efficient interface

* alexander.klemps@tuhh.de

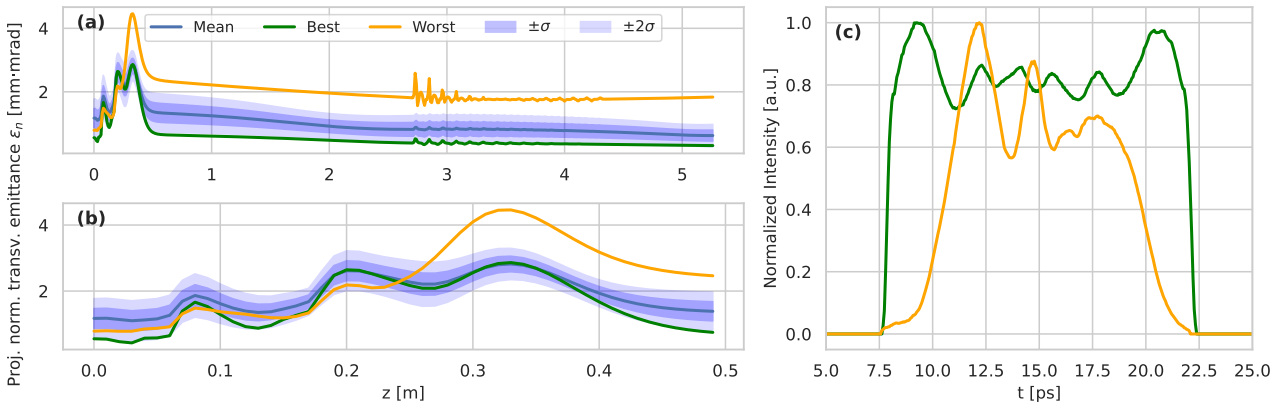

Figure 2: Evolution of the projected normalized transverse emittance ϵ_n along the PITZ beamline for varying longitudinal pulse shapes sampled from the latent space. (a) Emittance evolution over the full lattice. The mean trajectory (blue) is shown together with the corresponding $\pm 1\sigma$ and $\pm 2\sigma$ intervals (shaded), as well as the best (green) and worst (orange) cases in terms of final emittance. (b) Zoom into the near-cathode region ($z < 0.5$ m). (c) Corresponding normalized temporal profiles of the best and worst emittance evolutions.

for exploring pulse-induced effects and are used here as control parameters to study their impact on transverse emittance.

BEAM DYNAMICS SIMULATIONS

The accelerator lattice models the PITZ facility up to 5.28 m, covering the electron gun and CDS booster. This corresponds to the location of transverse emittance measurements in the PITZ setup [10], motivating the chosen simulation horizon. In total, 8500 beam dynamics simulations were performed using ASTRA [11], each with 2×10^4 macroparticles, providing a compromise between computational cost and resolution of projected beam properties.

Table 1: List of Beam Dynamics Simulation Parameters

Simulation Parameter	Value	Unit
Temporal pulse length (rms)	10	ps
Transverse laser spot size (rms)	0.2	mm
Main solenoid max. strength	0.21	T
Gun phase	0.67	deg
Gun frequency	1.3	GHz
Gun gradient	57.5	MV/m
Bunch charge	250	pC

Across all simulations, only the longitudinal laser pulse shape was varied using the WAE-based latent representation. Pulse shapes were intensity normalized and standardized to equal temporal rms lengths prior to simulation. Samples were generated by encoding pulse shapes from the dataset and performing linear interpolation in latent space, yielding a diverse set of physically plausible temporal profiles. These were decoded and used as input distributions for particle emission via inverse transform sampling.

To isolate the effect of pulse shape variation on transverse emittance, all remaining accelerator parameters, as well as the temporal pulse length and transverse laser spot size, were kept fixed at the values summarized in Table 1. The transverse laser profile at the photocathode was assumed to be radially symmetric and Gaussian.

RESULTS

The impact of longitudinal pulse shaping on transverse beam quality is evaluated by propagating the generated particle distributions through the PITZ lattice. Figure 2 shows the evolution of the normalized transverse emittance along the beamline for the considered pulse shapes, together with mean and standard deviation bands. While all configurations exhibit characteristic emittance growth in the near-cathode region followed by partial compensation, the final emittance at $z = 5.28$ m shows a substantial spread across the dataset. The mean final emittance is 0.621 mm mrad with a standard deviation of 0.17 mm mrad, and minimum and maximum values of 0.305 mm mrad and 1.833 mm mrad, respectively. Representative pulse shapes corresponding to the minimum and maximum final emittance are included in Fig. 2. The optimal pulse exhibits a relatively symmetric, flattop-like intensity profile, whereas the worst-performing case shows pronounced asymmetry and localized charge concentration.

Pearson correlations between latent variables and transverse emittance are used to quantify the relevance of individual dimensions. The resulting distributions (Fig. 3) show that only a subset of dimensions exhibits significant correlation, particularly downstream, indicating that beam quality is governed by a limited number of degrees of freedom in the latent space. In particular, dimensions ξ_{17} and ξ_{28} show strong correlation with the final emittance, while ξ_{22} exhibits moderate influence. Upon inspection, these directions can be qualitatively linked to pulse morphology: ξ_{17} governs flattop-to-peaked transitions, ξ_{28} controls multi-peak structure, and ξ_{22} affects fine-scale modulation. A partial least squares (PLS) projection is then applied to capture the combined effect of these variables. The variation in final transverse emittance is largely described by a low-dimensional subspace spanned by five components, explaining approxi-

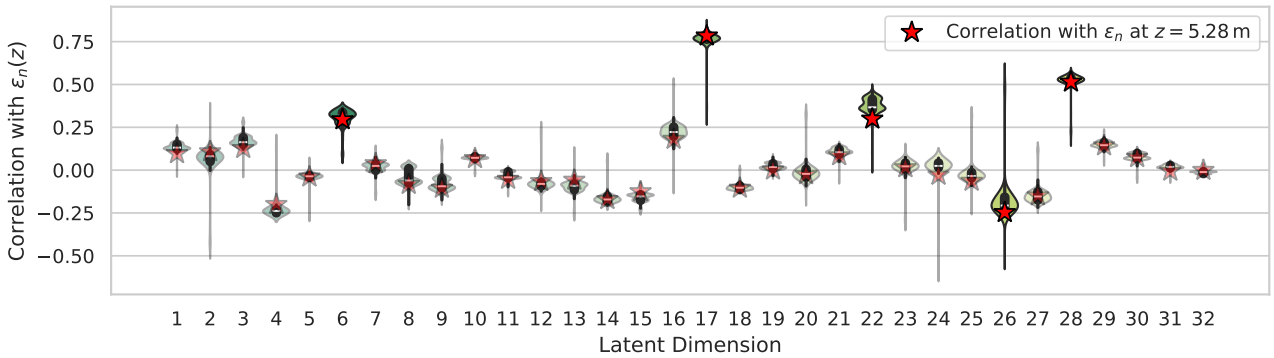

Figure 3: Pearson correlations ρ between latent coordinates of the WAE-encoded pulse shapes and the projected normalized transverse emittance ϵ_n. For each latent dimension, the violin plots show the distribution of correlations with $\epsilon_n(z)$ evaluated along the beamline. Red markers indicate the correlation with the $\epsilon_n(z = 5.28)$. Dimensions with weak final correlation ($|\rho| < 0.2$) are shown with reduced opacity.

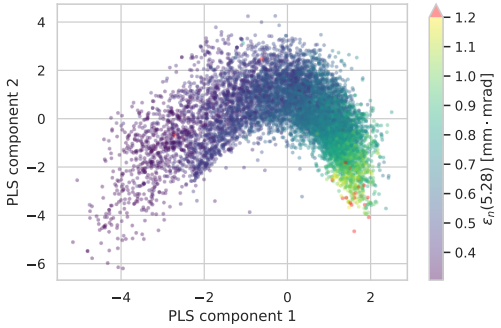

Figure 4: Projection of the latent pulse embeddings onto the first two PLS components, colored by the final transverse emittance at $z = 5.28$ m.

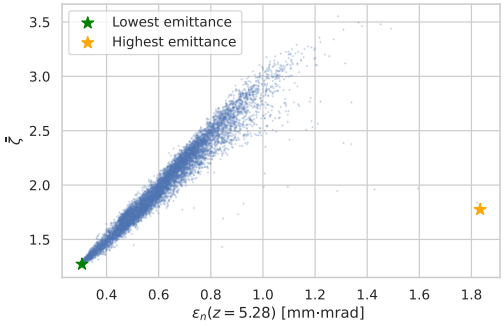

Figure 5: Current-weighted mean slice mismatch versus final projected transverse emittance.

mately 86% of the variance ($R^2 \approx 0.86$). The corresponding projection (Fig. 4) shows a monotonic variation of emittance along the leading component, indicating a dominant control direction in latent space.

While projected emittance is used as the primary beam-quality metric, slice mismatch at $z = 5.28$ m is additionally evaluated to characterize the internal phase-space consistency of the bunch. The beam is discretized into $N = 20$ slices indexed by $j \in \{1, \ldots, 20\}$, with corresponding slice currents I_j. The mismatch is defined as

$$\zeta_j = \frac{1}{2}\left(\beta_0\gamma_j - \alpha_0\alpha_j + \gamma_0\beta_j\right) \geq 1, \qquad \bar{\zeta} = \frac{\sum_{j=1}^{N} I_j\,\zeta_j}{\sum_{j=1}^{N} I_j},$$

where $(\alpha_j, \beta_j, \gamma_j)$ and $(\alpha_0, \beta_0, \gamma_0)$ denote slice and projected Twiss parameters, respectively.

A strong correlation between $\bar{\zeta}$ and the final projected emittance is observed (Fig. 5, $\rho(\bar{\zeta}, \varepsilon_n) \approx 0.96$), indicating that increased slice phase-space misalignment in populated regions of the bunch is consistently associated with higher emittance. At the same time, visible deviations from this trend suggest that mismatch alone does not fully determine beam quality in extreme cases. Overall, the results indicate that slice phase-space misalignment constitutes the dominant mechanism governing emittance variation across pulse shapes within our considered simulation setup.

CONCLUSION

Within this study, we demonstrate that a learned low-dimensional parameterization of longitudinal pulse shapes reveals that transverse emittance in the PITZ injector is effectively governed by a small number of shape degrees of freedom. The identified low-dimensional emittance-relevant subspace provides a suitable basis for training data-efficient surrogate models and enables Bayesian optimization strategies [12] for targeted exploration and optimization of beam emittance within a reduced and physically meaningful parameter space.

ACKNOWLEDGEMENTS

This work was supported by the German Federal Ministry of Research, Technology and Space under project OPAL-FEL, grant 05D23GT1. The authors thank the groups FS-LA and MXL at DESY and their project partners at PITZ.

REFERENCES

[1] Mahnke, Christoph *et al.*, "Novel photocathode lasers for the hard- and soft-x-ray free electron lasers euxfel and flash", *EPJ Web Conf.*, vol. 307, p. 04001, 2024. doi:10.1051/epjconf/202430704001

[2] D. Ilia *et al.*, "Novel photoinjector laser providing advanced pulse shaping for flash and euxfel", in *Proc. IPAC'25*, Taipei, Taiwan, Jun. 2025, pp. 2564–2567. doi:10.18429/JACoW-IPAC2025-THPB027

[3] D. Ilia, N. Ay, I. Hartl, W. Hillert, and H. Tünnermann, "Differentiable Models for Control of Complex Physical Systems: A Case Study in Laser Pulse Shaping", *NeurIPS Machine Learning and the Physical Sciences Workshop*, 2025.

[4] Y. C. et al., "Characterization of low-emittance electron beams generated by a new photocathode drive laser system nepal at the european xfel", in *Proc. IPAC'24*, Nashville, TN, pp. 388–391, May 2024. doi:10.18429/JACoW-IPAC2024-MOPG47

[5] A. Edelen and X. Huang, "Machine learning for design and control of particle accelerators: a look backward and forward", *Annual Review of Nuclear and Particle Science*, vol. 74, no. Volume 74, 2024, pp. 557–581, 2024. doi:10.1146/annurev-nucl-121423-100719

[6] J. Wan, J. Qiang, and Y. Hao, "Symplectic machine learning model for fast simulation of space-charge effects", *Phys. Rev. Accel. Beams*, vol. 28, no. 7, p. 074602, Jul. 2025. doi:10.1103/bhpv-bcqk

[7] 2018. https://openreview.net/forum?id=HkL7n1-0b

[8] A. Klemps, D. Ilia, P. K. Banerjee, Y. Chen, H. Tünnermann, and N. Ay, "Learning a latent pulse shape interface for photoinjector laser systems", 2026, doi:10.48550/arXiv.2602.17263,

[9] D. Ilia and A. Klemps, "OPAL-FEL EuXFEL NEPAL Frontend Simulation Data", Zenodo, Apr. 2025, doi:10.5281/zenodo.15125336,

[10] A. Hoffmann, S. Zeeshan, J. Good, M. Gross, M. Krasilnikov, and F. Stephan, "Efficient generation of transversely and longitudinally truncated chirped gaussian laser pulses for application in high-brightness photoinjectors", *Photonics*, vol. 12, no. 5, 2025. doi:10.3390/photonics12050460

[11] K. Floettmann, ASTRA - A Space Charge Tracking Algorithm, 1997. https://www.desy.de/~mpyflo/

[12] R. Roussel *et al.*, "Bayesian optimization algorithms for accelerator physics", *Phys. Rev. Accel. Beams*, vol. 27, no. 8, p. 084801, Aug. 2024. doi:10.1103/PhysRevAccelBeams.27.084801